Cornell CBN 97–13
May 8, 1997

A Luminosity Monitor Using the Coherent Beam–Beam Interaction* (Internal Report)

D. Sagan, J. Sikora and S. Henderson
Laboratory of Nuclear Studies, Cornell University, Ithaca, NY 14853

Abstract

A new method of monitoring the luminosity has been developed at CESR. The method involves shaking one bunch at a specific frequency and observing the resulting oscillations of the corresponding opposing bunch. In initial tests, measurements with 1% accuracy have been obtained in 1 second. Measurements of different bunches in a train shows bunch to bunch differences with the optimum luminosity conditions for one bunch not coinciding with the optimum for another.

1 Introduction

In a colliding beam storage ring it is essential to be able to monitor the luminosity so as to be able to adjust machine elements (magnets, separators, etc.) to maximize the luminosity. Two methods that are used at the Cornell Electron/positron Storage Ring CESR involve measuring the vertical σ–π tune split and counting babas using the CLEO detector. The problem with the former method is that the π mode is not always cleanly visible on a spectrum analyzer. On the other hand, the latter method is slow since the counting rates are low—the characteristic time scale for a measurement being a minute.

With these problems in mind an alternative method has been developed that uses the coherent beam–beam interaction: A given bunch of one beam is shaken vertically. This "shaker" bunch interacts with a bunch of the opposite beam (called the "detected" bunch) at the interaction point (IP). The oscillations of the detected bunch are monitored and the amplitude of oscillation of the detected bunch is a measure of the luminosity. This Beam–Beam Interaction (BBI) luminosity monitor has proved to have several advantages: The hardware requirements are minimal and

*An abridged version of this paper has been submitted to the 1997 Particle Accelerator Conference.

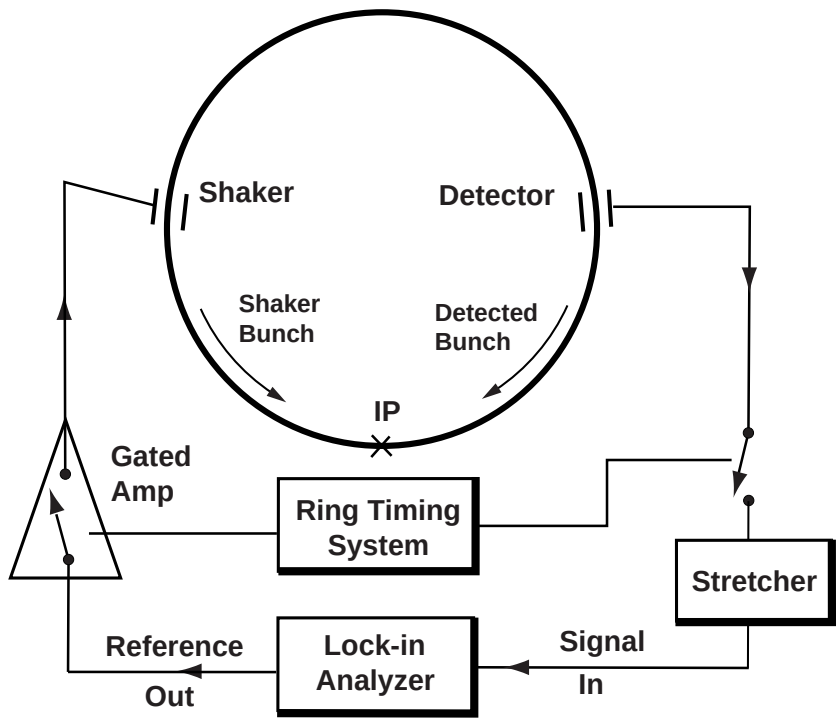

Figure 1: Schematic diagram of the BBI luminosity monitor configuration.

the response is fast with the characteristic time scale for a measurement being about a second. An added benefit is that with multiple bunches in each beam it is possible to individually monitor the luminosity of any given pair of bunches.

2 Theory

The configuration of the BBI luminosity monitor is shown schematically in figure 1. The sinusoidal reference signal at frequency ω_s from a lock–in amplifier is used to vertically shake a given bunch of a given beam with some amplitude $A'_s(\mathrm{sh})$. This shaker bunch is given a kick $\Delta y'_s$ of

$$\Delta y'_s = A'_s(\mathrm{sh}) \cdot \cos \omega_s t \; . \tag{1}$$

At the IP the shaking translates into an oscillation of the shaker bunch with amplitude $A_s(\mathrm{ip})$ given by

$$A_s(\mathrm{ip}) = A'_s(\mathrm{sh}) \sqrt{\beta_y(\mathrm{sh})\, \beta_y(\mathrm{ip})}\, F_{sh} \; , \tag{2}$$

where F_{sh} is the transfer function from the shaker to the IP. Formulas for F_{sh} are derived in appendix A. A necessary condition for the shaking not to affect the luminosity is

$$A_s(\mathrm{ip}) \ll \sigma_y \; , \tag{3}$$

where σ_y is the vertical beam size at the IP (For compactness all beam sizes refer to the IP unless explicitly shown otherwise).

At the IP the oscillations of the shaker bunch give a kick to the detected bunch. The amplitude of this kick, $A'_d(\mathrm{ip})$, is

$$A'_d(\mathrm{ip}) = \left|\frac{dy'}{dy}\right|_{y_{ds}} \cdot A_s(\mathrm{ip}) \ , \tag{4}$$

where dy'/dy is the derivative of the beam-beam kick which is evaluated at y_{ds}, with y_{ds} being the vertical offset between the centers of the two bunches when there is no shaking. For head–on collisions

$$\left|\frac{dy'}{dy}\right|_0 = \frac{4\pi\kappa\xi_y}{\beta_y(\mathrm{ip})} \ , \tag{5}$$

where ξ_y is the beam–beam tune shift parameter. If we were only dealing with particles near the core of the bunches then the correction factor κ in Eq. (5) would be 1. However, since it is the centroid motion that is measured, and since particles away from the core receive less of a kick, κ is less than 1. Measurements and calculation[1] give $\kappa \approx 0.6$ and this will be the value used for this paper. ξ_y can be related to the beam sizes through the standard formula

$$\xi_y = \frac{N_p \beta_y(\mathrm{ip}) r_e}{2\pi\gamma\sigma_y(\sigma_x + \sigma_y)} \ , \tag{6}$$

with N_p being the number of particles in a bunch, γ is the standard relativistic factor, and r_e the classical electron radius. ξ_y can also be related to the luminosity by

$$\mathcal{L} = \frac{\gamma I \xi_y}{2 e r_e \beta_y(\mathrm{ip})}(1 + r) \ , \tag{7}$$

where e is the electron charge, I the beam current, and $r \equiv \sigma_y/\sigma_x$.

From the kick given to the detected bunch the amplitude of oscillation $A_d(\mathrm{det})$ of the detected bunch at the detector is

$$A_d(\mathrm{det}) = A'_d(\mathrm{ip})\sqrt{\beta_y(\mathrm{ip})\beta_y(\mathrm{det})}\, F_{det} \ , \tag{8}$$

where F_{det} is the transfer function from the IP to the detector. Combining Eqs. (2), (4), (5), and (8) gives

$$A_d(\mathrm{det}) = \begin{cases} A'_s(\mathrm{sh})\,\beta_y(\mathrm{ip}) \left|\frac{dy'}{dy}\right|_{y_{ds}} \sqrt{\beta_y(\mathrm{sh})\beta_y(\mathrm{det})}\, F_{sh}\, F_{det} & \text{In general} \\ 4\pi A'_s(\mathrm{sh})\,\kappa\xi_y \sqrt{\beta_y(\mathrm{sh})\beta_y(\mathrm{det})}\, F_{sh}\, F_{det} & y_{ds} = 0 \end{cases} \tag{9}$$

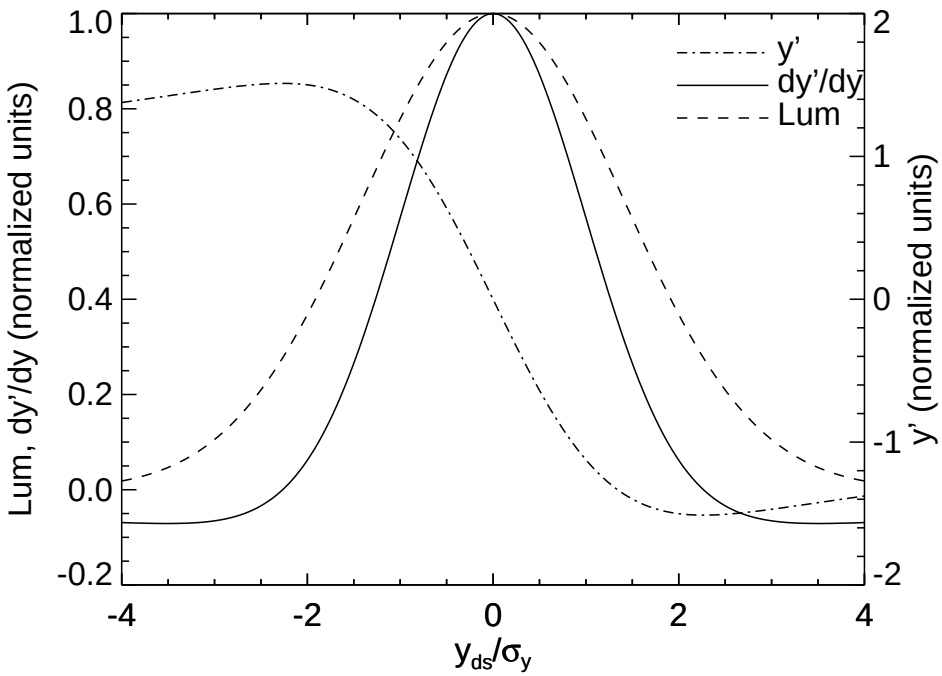

Figure 2: $\mathcal{L}$, dy'/dy, and y' as a function of y_{ds}/σ_y for $\sigma_y/\sigma_x = 0.1$. $\mathcal{L}$ and dy'/dy have been scaled to be 1 at $y_{ds} = 0$.

Eq. (9) is not quite correct since the effect of the detected bunch upon the shaker bunch has been neglected. However, since this effect is small ($< 10\%$) for CESR it will be ignored.

The signal from the detected bunch is stretched and held for a turn until the next signal is received (cf. Appendix B). The stretched signal is measured by the lock–in amplifier (cf. figure 1). In order to prevent unwanted interference, the shaker is gated so as to only kick the shaker bunch. Additionally, the signal from the BPM is gated to exclude the direct signal from the shaker bunch.

With multiple bunches in each beam, the oscillations of the shaker bunch may also be transmitted to the detected bunch via intermediate bunches that communicate through the long range BBI at the parasitic crossing points. This can be analyzed in a manner similar to the above analysis for the IP. The difference is that for the parasitic crossing points the long range ξ_y is an order of magnitude smaller than ξ_y at the IP. Because of this, and because the signal transmitted through the long range BBI is relatively insensitive to variations in machine parameters, this effect can be ignored.

From Eqs. (6), (7), and (9), for head–on collisions with flat beams

$$A_d(\mathrm{det}) \propto \xi_y \propto \beta_y(\mathrm{ip}) \cdot \mathcal{L} \propto \frac{\beta_y(\mathrm{ip})}{\sigma_x \sigma_y} \,. \tag{10}$$

Parameter	Value	Parameter	Value
I	6 ma	N_p	10^{11}
$\bar{\delta}$	10^{-4}	C	10 pF
ω_s	$2\pi \cdot 100\,\mathrm{kHz}$	ω_{rev}	$2\pi \cdot 390\,\mathrm{kHz}$
$A'_s(\mathrm{sh})$	0.5 μrad	σ_z	1.8 cm
ξ_y	0.03	N_s	$4 \cdot 10^5$
Q_y	9.596	t_1	1 sec
$\beta_y(\mathrm{ip})$	0.019 m	$\partial\epsilon_{bpm}/\partial y$	0.64/m
$\sigma_y(\mathrm{ip})$	7 μm	$\sigma_y(\mathrm{det})$	300 μm
$\beta_y(\mathrm{sh})$	21.5 m	$\beta_y(\mathrm{det})$	32.3 m
$\phi_y(\mathrm{sh})$	$2\pi \cdot 0.86$	$\phi_y(\mathrm{det})$	$2\pi \cdot 0.27$
F_{sh}	0.79	F_{det}	0.82

Table 1: CESR BBI luminosity monitor parameters. The shaker is KVH10W1 and the detector is DT02W2.

Thus, the BBI luminosity monitor can be use to adjust skew quadrupoles to minimize σ_y and maximize $\mathcal{L}$. However, because of the factor of $\beta_y(\mathrm{ip})$ in Eq. (10), the BBI luminosity monitor cannot be used to adjust $\beta_y(\mathrm{ip})$ since it is possible to increase $A_d(\mathrm{det})$ by increasing $\beta_y(\mathrm{ip})$ while simultaneously decreasing $\mathcal{L}$. This drawback is also inherent when using the σ–π tune split as a measure of the luminosity since the σ–π tune split also is essentially proportional to ξ_y.

Figure 2 shows y', dy'/dy, and $\mathcal{L}$ as a function of y_{ds}/σ_y with dy'/dy and $\mathcal{L}$ being normalized to 1 at $y_{ds} = 0$. In the figure, the kick y' was calculated using the standard Bassetti and Erskine complex error function formula (cf Talman[1]). For $|y_{ds}| \lesssim 2\sigma_y$, dy'/dy tracks $\mathcal{L}$ with maximum $\mathcal{L}$ coinciding with maximum dy'/dy at $y_{ds} = 0$. The BBI luminosity monitor can thus be used to adjust machine elements to obtain head–on collisions.

3 CESR BBI Luminosity Monitor

The CESR BBI Luminosity is piggybacked on the transverse feedback system[2]. An analysis of the detector electronics is given in appendix B. "Typical" values for the parameters of the CESR BBI luminosity monitor are given in table 1[3]. The shaking frequency is chosen at the upper end of the lock–in amplifier range to get maximum effect since $A'_s(\mathrm{sh})$ is limited to the value given in table 1 by the shaker power amplifier. In any case, the shaking frequency should be kept well away from any betatron resonance sideband so that changes in the betatron frequency do not result in large changes in the measured signal. With the numbers in table 1, and

using Eqs. (22) and (23), F_{sh} and F_{det} are as given in table 1. From Eq. (2), $A_s(\mathrm{ip})$ is

$$A_s(\mathrm{ip}) = 0.25\,\mu\mathrm{m}\ . \tag{11}$$

This is 4% of σ_y so Eq. (3) is satisfied. Using Eq. (9) with $y_{ds} = 0$ gives

$$A_d(\mathrm{det}) = 1.9\,\mu\mathrm{m}\ . \tag{12}$$

Using this in Eq. (27) gives the lock–in voltage signal

$$V_{sig} = 1400\,\mu\mathrm{V}\ . \tag{13}$$

Initial measurements gives $V_{sig} = 200\,\mu\mathrm{V}$. This is with a 10 dB attenuator before the buffer to prevent overloading (cf. figure 6) and with the two top and the two bottom buttons cowed together. Without the attenuator, and the cowing, the signal would be $V_{sig} = 500\,\mu\mathrm{V}$. Considering the crudeness of the model of the detector electronics, the factor of 3 difference between the calculation of $1400\,\mu\mathrm{V}$ and measurement of $500\,\mu\mathrm{V}$ is not unreasonable. A contributing factor to the difference is the attenuation in the cable which was not taken into account. Another problem is that the capacitance shown in figure 6 is due to the parasitic front end capacitance of the buffer and therefore the value listed in table 1 is only an estimate.

For a given desired accuracy, the signal–to-noise ratio of the system will determine the minimum time it takes to do a measurement. Consider first the noise on the beam centroid motion due to radiation fluctuations. This is derived in appendix C. Using the values in Table 1, and Eq. (36) for the noise far from resonance, the RMS noise in the vertical motion is

$$\sigma_{ny}(\mathrm{det}) \approx 1 \cdot 10^{-8}\,\mu\mathrm{m}\ . \tag{14}$$

This is very small compared to the shaking amplitude $A_d(\mathrm{det})$ given by Eq. (12). The radiation noise is thus not a factor that limits the measurement.

For the filter employed by the lock–in (n cascaded RC filters, all with the same time constant, with n between 1 and 4) the time t_1 for the response to settle to within 1% of its final value after a step change in signal is related to the noise bandwidth $\Delta f_n(\text{lock–in})$ by

$$\Delta f_n(\text{lock–in}) \simeq \frac{1}{t_1}\ . \tag{15}$$

For a 1% settling time, if we want the voltage noise at the lock–in, σ_{nV}, to be some fraction r_n of the signal V_{sig} then, from Eq. (15), the ratio of noise per unit bandwidth to signal is

$$\frac{\sigma_{nV}/\sqrt{\Delta f_n(\text{lock–in})}}{V_{sig}} = r_n\sqrt{t_1}\ . \tag{16}$$

Using Eq. (31) of appendix B, and using the values in table 1, the noise per unit bandwidth due to the beam button load resistor is

$$\frac{\sigma_{nV}}{\sqrt{\Delta f_n(\text{lock–in})}} = 0.2\,\mu\mathrm{V}/\sqrt{\mathrm{hz}}\ . \tag{17}$$

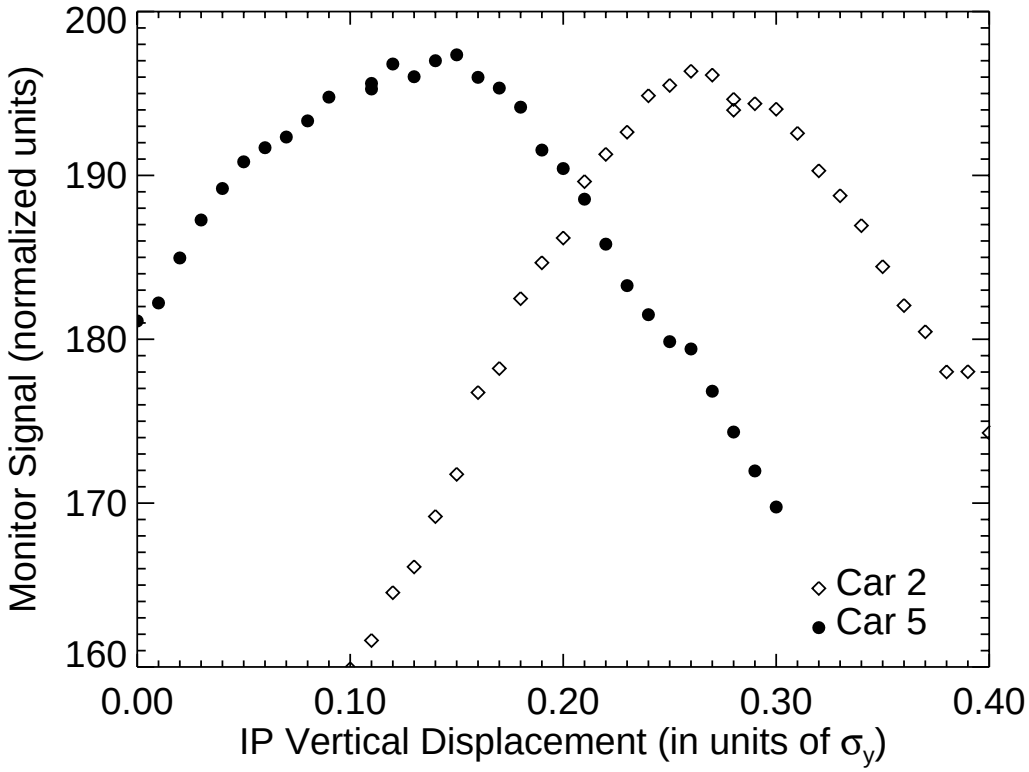

Figure 3: Monitor signals for car 2 and car 5 as a function of vertical displacement of the bunches.

Thus, with a 500 μV signal, the "ultimate" noise per unit bandwidth to signal ratio is $4 \cdot 10^{-4}/\sqrt{\mathrm{hz}}$ which would, for example, give a 1% settle time of 0.2 seconds with a noise–to–signal of 1%. In an initial test using using the COMET system as the detector, the measured noise per unit bandwidth to signal ratio was $0.01/\sqrt{\mathrm{hz}}$ which is equivalent to a 1 second settling time with 1% noise–to–signal.

4 Experimental Results

Initial tests were done using HEP conditions with 2 cars (#2 and #5) filled per train with the spacing between cars being 42 nsec. There were 9 trans per beam with a 280 nsec to 294 nsec spacing between trains. The vertical differential orbit through the IP was varied using an electrostatic bump ("VCROSING 7"). Figure 3 shows the monitor signals from car 2 and car 5 of train 1 as a function of separation at the IP. The monitor signals have been normalized by the total beam current. The vertical separation is calibrated in units of the nominal σ_y (7 μm) appropriate for the observed luminosity. Thus, from one end of the plot to the other, the change in y_{ds} is $0.4\sigma_y$. The fact that the peaks of the two signals do not coincide implies that the cars are

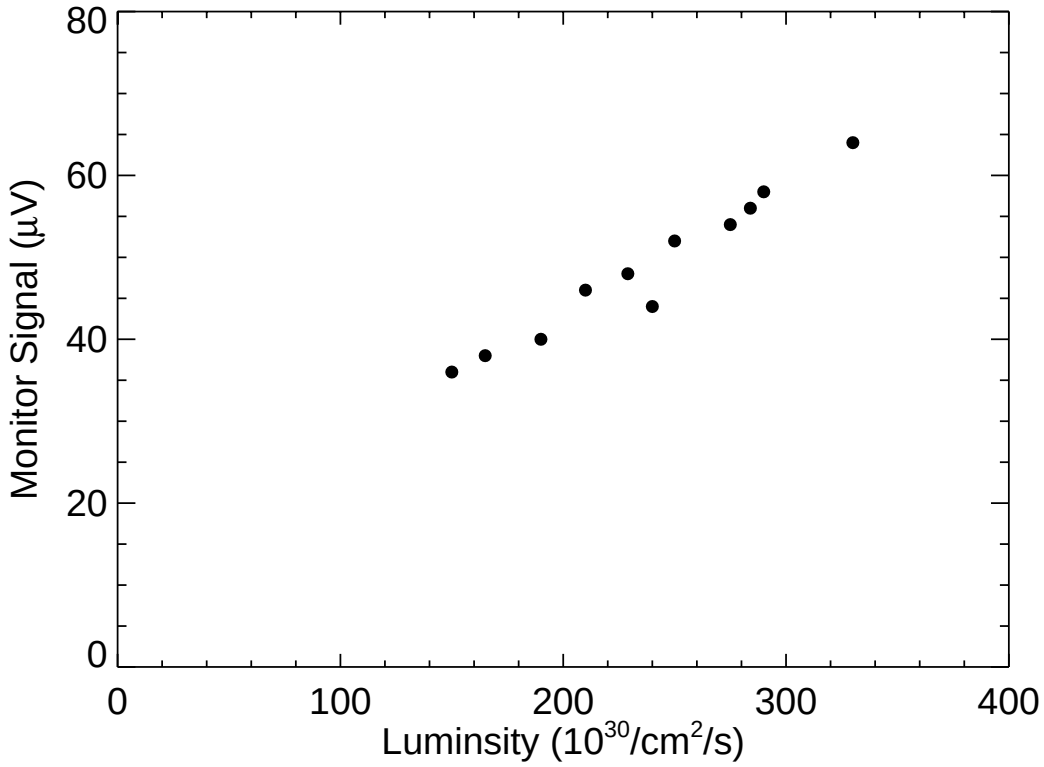

Figure 4: Car 2 monitor signal as a function of CLEO luminosity while varying y_{ds}.

not following the same vertical trajectory. The leading suspect to explain this is the short range wake fields produced by the leading (#2) car.

The width of the monitor signal shown in figure 3 for car 2 or car 5 is substantially less than what one would expect from figure 2. This is not surprising since the curves in figure 2 were calculated assuming a constant beam size. However, with the beams colliding off–center, resonances will be excited through the beam–beam interaction that would be excluded in the head–on case through symmetry. This will lead to beam blowup and hence greater sensitivity to y_{ds}. Indeed, a measurement of the car 2 monitor signal as a function of the luminosity measured by the CLEO detector while varying y_{ds}, shown in figure 4, shows a linear relationship. This would be appropriate for variations in σ_y (cf. Eq. (10)), but is not what would be predicted from figure 2.

Another noteworthy feature in figure 3 is that the width of the car 5 curve is greater than the width of the car 2 curve. One possible explanation is that since the car 5 data was taken after the car 2 data the beam current is less. Hence, with the car 5 data, there is less of a beam–beam interaction so that the car 5 curve looks more like figure 2. Another possibility could involve the short range wake fields. More experimentation will resolve this issue.

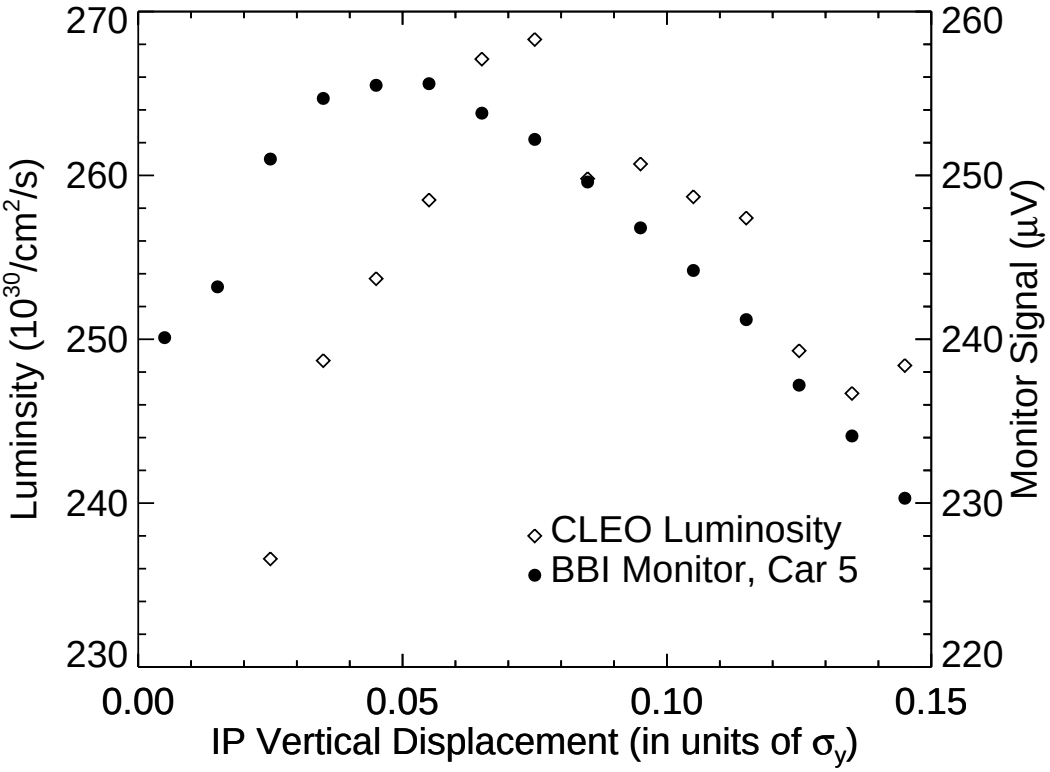

Figure 5: Monitor signal for car 5 and CLEO luminosity as a function of vertical displacement of the bunches.

Figure 5 shows the CLEO luminosity and the car 5 monitor signal again as a function of relative vertical displacement at the IP. Comparing with figure 3 the luminosity peak falls between the car 2 and car 5 peaks as expected. However, the luminosity peak is not centered—the separation between the car 5 and the luminosity peaks is only 25% the separation between the car 2 and car 5 peaks. One possible explanation for this discrepancy is that since it took a relatively long time to take the data used in figure 4 (the CLEO luminosity signal takes ~2 minutes to respond to any changes) there might have been a shift in machine conditions during the data taking that caused a movement of the apparent peak separation. Again more experimentation will resolve the issue.

5 Conclusion

Using the coherent beam-beam interaction to monitor the luminosity has several clear advantages: The system has a fast response time so tuning of machine elements can be done efficiently by an operator or a computer program. The system is also easy to construct—the necessary shaker and detector hardware are typical of any storage

ring and the external electronics is minimal. Additionally, bunch to bunch variations in the luminosity can be monitored. The one significant drawback is that it is not possible to use the BBI luminosity monitor to optimize the beta at the IP.

Acknowledgements

Our thanks to Bob Meller, Mike Billing, and Don Hartill for useful discussions, and to Gerry Codner for help with the electronics. Thanks also must be given Elizabeth Young and Richard Talman whose work on measuring the beam–beam kick was the inspiration for the present work.

Appendix A: Response to a shaker

The object is to calculate the beam oscillations induced by a shaker. [This has undoubtedly been derived many times before. However, since I do not have a good reference for this, I derive it here for posterity.] The coordinates (y, y') of the beam can be described using a complex number z

$$z \equiv y - iy'\beta_y \,. \tag{18}$$

Without shaking, $z(s,n)$—the coordinates on turn n and at longitudinal position s—is related to $z(0,m)$ by

$$z(s,n) = z(0,m)\sqrt{\frac{\beta_y(s)}{\beta_y(\mathrm{sh})}}\, e^{i\bar{\omega}_y p}\, e^{-\bar{\delta}p}\, e^{i\phi_y(s)} \,, \tag{19}$$

where $\phi_y(s)$ is the phase advance from the shaker (taken here to be at $s = 0$) to position s and

$$\begin{aligned} \bar{\omega}_y &\equiv 2\pi\omega_y/\omega_{rev} \,, \quad \text{and} \\ \bar{\delta} &\equiv 2\pi\delta/\omega_{rev} \,. \end{aligned} \tag{20}$$

In Eq. (20) ω_y is the betatron frequency, δ is the damping decrement, and ω_{rev} is the revolution frequency. Using Eqs. (1) and (18) the kick $\delta z(m)$ given by the shaker on turn m is

$$\delta z(m) = -iA_s'(\mathrm{sh})\,\beta_y(\mathrm{sh})\cos(\bar{\omega}_s m) \,, \tag{21}$$

where $\bar{\omega}_s \equiv 2\pi\omega_s/\omega_{rev}$. With the skaker turned on, $z(s,n)$ can be written as the sum of the displacements due to the kicks on all the previous turns

$$\begin{aligned} z(s,n) &= -i\,A_s'(\mathrm{sh})\sqrt{\beta_y(s)\,\beta_y(\mathrm{sh})}\sum_{m=-\infty}^{n}\cos(\bar{\omega}_s m)\,e^{i\bar{\omega}_y(n-m)}\,e^{-\bar{\delta}(n-m)}\,e^{i\phi_y(s)} \\ &= \frac{-i\,A_s'(\mathrm{sh})\sqrt{\beta_y(s)\,\beta_y(\mathrm{sh})}}{2}\left[\frac{e^{i(\bar{\omega}_s n+\phi_y(s))}}{1-e^{i(\bar{\omega}_y-\bar{\omega}_s)}\,e^{\bar{\delta}}} + \frac{e^{i(-\bar{\omega}_s n+\phi_y(s))}}{1-e^{i(\bar{\omega}_y+\bar{\omega}_s)}\,e^{\bar{\delta}}}\right] \,. \end{aligned} \tag{22}$$

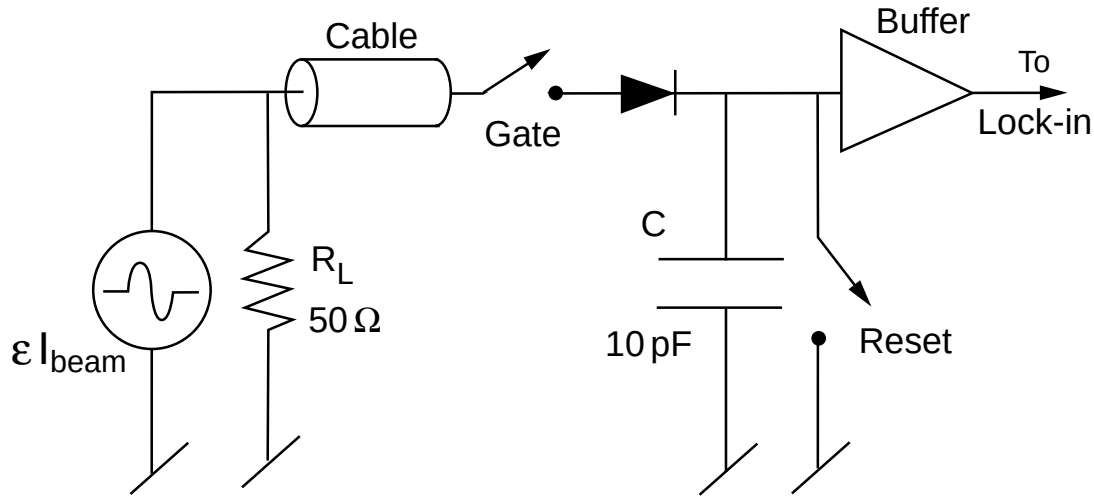

Figure 6: Model circuit for the BPM front end.

The position y is given by the real part of $z(s,n)$. From Eq. (22), y can be written in the form

$$y = \mathrm{Re}\,[z(s,n)] = A'_s(\mathrm{sh})\sqrt{\beta_y(s)\,\beta_y(\mathrm{sh})}\,F(\phi_y(s),\bar{\omega}_s,\bar{\omega}_y,\bar{\delta})\cdot\cos(\bar{\omega}_s n+\theta_s)\,. \tag{23}$$

Eq. (23) defines the transfer function F. There are three principle cases where F assumes a simple form:

$$F = \begin{cases} \dfrac{\cos\left(\bar{\omega}_y/2-\phi_y(s)\right)}{2\sin\bar{\omega}_y/2} & \bar{\omega}_s \ll 1 \text{ and } \bar{\omega}_s \ll \bar{\omega}_y. \\ \dfrac{1}{2\sqrt{\bar{\delta}^2+(\bar{\omega}_s-\bar{\omega}_y-k)^2}} & \bar{\omega}_s \approx \bar{\omega}_y + k,\ k \text{ an integer} \\ \dfrac{1}{2\sqrt{\bar{\delta}^2+(\bar{\omega}_s+\bar{\omega}_y-k)^2}} & \bar{\omega}_s \approx -\bar{\omega}_y + k,\ k \text{ an integer} \end{cases} \tag{24}$$

For the low frequency case F has the same form as a static orbit bump.

Appendix B: Signal and Noise for a the Detector Electronics

The model circuit for the detector system is shown in figure 6. The bipolar signal from a button electrode is split between a load resistor R_L (used for circuit protection and to prevent multiple reflections) and a coaxial cable. Only the signal from the correct bunch is allowed to pass through the gate. The signal is rectified and the positive going part is used to charge a capacitor. The voltage on the capacitor is

sampled by the lock–in via a buffer amplifier. The charge on the capacitor is held for almost a turn. Just before the next signal, the capacitor is drained by the reset gate and the process is repeated. In order to double the signal two circuits are used. One with a top, and the other with a bottom button electrode. The lock–in then takes the difference between the two.

The signal from the beam is a bipolar pulse. As long as $\sigma_z \lesssim D$ (where D is the diameter of the button electrode) the positive going part of the signal can be approximated by

$$I_{signal} \approx \epsilon_{bpm} I_{beam} \ , \tag{25}$$

where ϵ_{bpm} is a geometric factor dependent upon the chamber and monitor electrode geometry, and upon the position of the beam. Assuming that half the signal is absorbed by the load resistor and that the other half charges the capacitor, the voltage V_c on the capacitor is

$$V_c = \frac{\epsilon_{bpm} N_p e}{2C} \ , \tag{26}$$

where C is the capacitance. The RMS voltage signal V_{sig} due to vertical oscillations in the beam is then

$$V_{sig} = \frac{N_p e}{C} \cdot \frac{\partial \epsilon_{bpm}}{\partial y} \cdot \frac{A_d(\mathrm{det})}{\sqrt{2}} \ , \tag{27}$$

where a factor of $\sqrt{2}$ comes from converting peak amplitude to RMS and another factor of 2 comes from using the difference signal from two buttons.

The RMS noise voltage on the capacitor due to the load resistor is

$$\sigma_{nV}^2(cap) = 4 k_B T R_L \Delta f_n(cap) \ , \tag{28}$$

where k_B is Boltzmann's constant, T is the temperature, and $\Delta f_n(cap)$ is the noise bandwidth at the capacitor. $\Delta f_n(cap)$ is related to the charging time t_c of the capacitor by

$$\Delta f_n(cap) \approx \frac{1}{t_c} \approx \frac{c}{2\sigma_z} \ . \tag{29}$$

For the lock–in, since the signal is changing once per turn, the effective number of samples N_s is related to the lock–in noise bandwidth by $\Delta f_n(\text{lock–in})$

$$N_s \simeq \frac{\omega_{rev}}{2\,\pi\,\Delta f_n(\text{lock–in})} \ . \tag{30}$$

Since the lock–in samples N_s times the noise on the output from the lock–in will be reduced by $\sqrt{N_s}$. From Eqs. (28) and (29), for a 50Ω load resistance the lock–in output signal will thus have an RMS noise of

$$\sigma_{nV} \approx \frac{0.91\,\mathrm{nV}}{\sqrt{\mathrm{hz}}} \sqrt{\frac{c}{\sigma_z\, N_s}} \ , \tag{31}$$

where an extra factor of $\sqrt{2}$ comes from using the difference signal from two buttons.

Appendix C: Beam Centroid Noise Due to Radiation Fluctuations

We want to calculate the intrinsic noise spectrum in the centroid motion of the beam. [Again, this undoubtedly has been derived before. However, having no reference, I derive it yet again.] Consider first a single particle. The transverse position of the particle will be described using z as defined in Eq. (18). If the position is sampled N_s times then the measured noise signal $z_n(\bar{\omega}_s)$ at frequency $\bar{\omega}_s$ is

$$z_n(\omega_s) = \frac{1}{N_s} \sum_{m=1}^{N_s} z_n(m) e^{-i\bar{\omega}_s m} , \tag{32}$$

where $z_n(m)$ is noise on the mth sample (This assumes that both y and y' are measured. If only y is measured then the real part must be taken in Eq. (32)).

Over 1 turn radiation excitation will kick the particle by z_{rad}. The oscillations resulting from this kick is given by Eq. (19). The contribution z_{n1} to the sum in Eq. (32) due to a single kick is

$$\begin{aligned} z_{n1} &= \frac{1}{N_s} \sum_m z_{rad}\, e^{i\bar{\omega}_y m}\, e^{-\bar{\delta} m}\, e^{i\bar{\omega}_s m} \\ &= \frac{z_{rad}}{N_s} \left[\frac{1}{1 - e^{i(\bar{\omega}_y - \bar{\omega}_s)} e^{-\bar{\delta}}} \right] , \end{aligned} \tag{33}$$

where it is assumed that $N_s \gg 1/\bar{\delta}$. The RMS amplitude of the radiation kick is (Cf. Sands[4], chapter 5)

$$\left\langle |z_{rad}|^2 \right\rangle \approx \bar{\delta} \cdot \sigma_y^2(\text{det}) , \tag{34}$$

where $\bar{\delta}$ is given by Eq. (20) and $\sigma_y(\text{det})$ is the sigma at the detector. Since the radiation kicks are uncorrelated the contributions of the individual kicks add in quadrature. Additionally, the contributions of the N_p particles of the bunch are uncorrelated and add in quadrature. Thus, the RMS of the noise signal, σ_{ny}, in the centroid motion due to the N_s radiation kicks which occur during the sampling period is from Eqs. (33) and (34)

$$\sigma_{ny}^2(\omega_s) \equiv \left\langle z_n^2(\omega_s) \right\rangle \approx \frac{\bar{\delta}\sigma_y^2}{N_p N_s |1 - e^{i(\bar{\omega}_y - \bar{\omega}_s)}|^2} \tag{35}$$

There are two principal cases of interest:

$$\sigma_{ny}^2(\omega_s) \approx \begin{cases} \dfrac{\bar{\delta}\sigma_y^2}{N_p N_s (\bar{\delta}^2 + (\bar{\omega}_s - \bar{\omega}_y - k)^2)} & \bar{\omega}_s \approx \bar{\omega}_y + k,\ k \text{ an integer} \\ \dfrac{\bar{\delta}\sigma_y^2}{N_p N_s} & \text{Far from resonance} \end{cases} \tag{36}$$

References

[1] R. Talman, "Multiparticle Phenomena and Landau Damping," in AIP Conf. Proc. **153** pp. 789–834, M. Month and M. Diens editors, American Institute of Physics, New York (1987). K. Yokoya and H. Koiso, "Tune Shift of Coherent Beam–Beam oscillations," Part. Acc. **27** pp. 181-86, (1990).

[2] J. T. Rogers, M. G. Billing, J. A. Dobbins, et. al, "Operation of a Fast Digital Transverse Feedback System in CESR," Proc. 1995 Part. Acc. Conf., p. 2426 (1995).

[3] Value for $\partial\epsilon_{bpm}/\partial y$ is obtained from a paper by Mike Billing "Calculation of Beam Position Detector Parameters," 7/4/80.

[4] Matthew Sands, *The Physics of Electron Storage Rings, An Introduction*, SLAC-121 Addendum, (1970).